Supporting Information

Manipulation of Morphologies and Magnetic Properties for $Bi_{4.2}K_{0.8}Fe_2O_{9+\delta}$ Nanostructures

Sining Dong, Yukuai Liu, Shengwei Yang, Tao Jiang, Yuewei Yin and Xiaoguang Li*

Hefei National Laboratory for Physical Sciences at Microscale, Department of Physics, CAS Key Lab Mat Energy Convers, University of Science and Technology of China, Hefei 230026, P. R. China

* E-mail: lixg@ustc.edu.cn

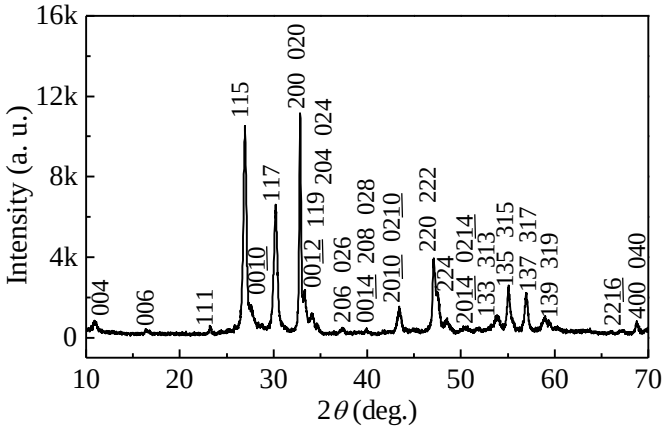

Fig. S1. XRD pattern of the urchin-like $Bi_{4.2}K_{0.8}Fe_2O_{9+\delta}$ samples obtained at T_{KOH} = 50 °C and T_{HT} = 90 °C.

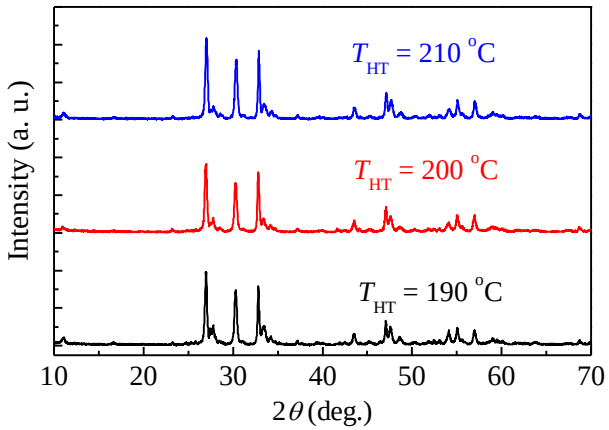

Fig. S2. XRD patterns of the $Bi_{4.2}K_{0.8}Fe_2O_{9+\delta}$ samples obtained at T_{KOH} = 50 °C and different T_{HT} (T_{HT} = 190 °C, 200 °C and 210 °C).

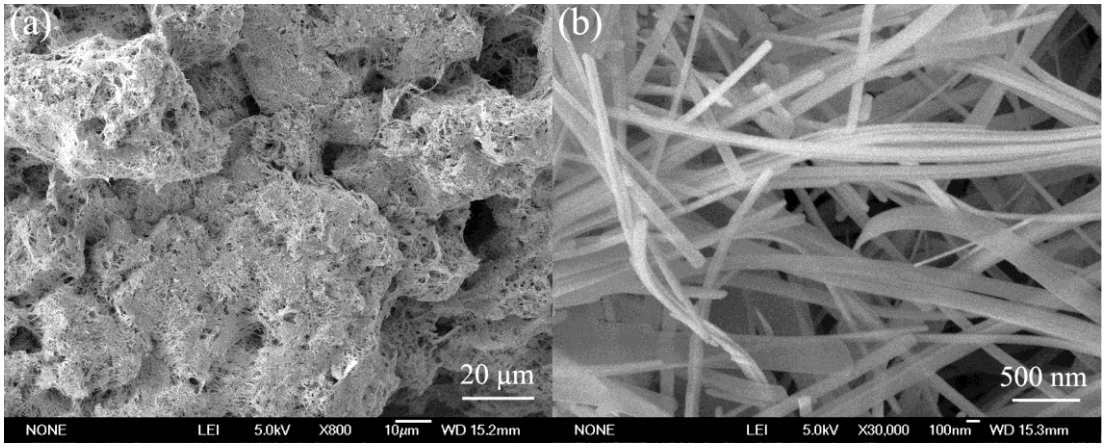

Fig. S3. (a) Low- and (b) high-magnification FESEM images of the $Bi_{4.2}K_{0.8}Fe_2O_{9+\delta}$ samples obtained at T_{KOH} = 50 ^{o}C and T_{HT} = 210 ^{o}C.

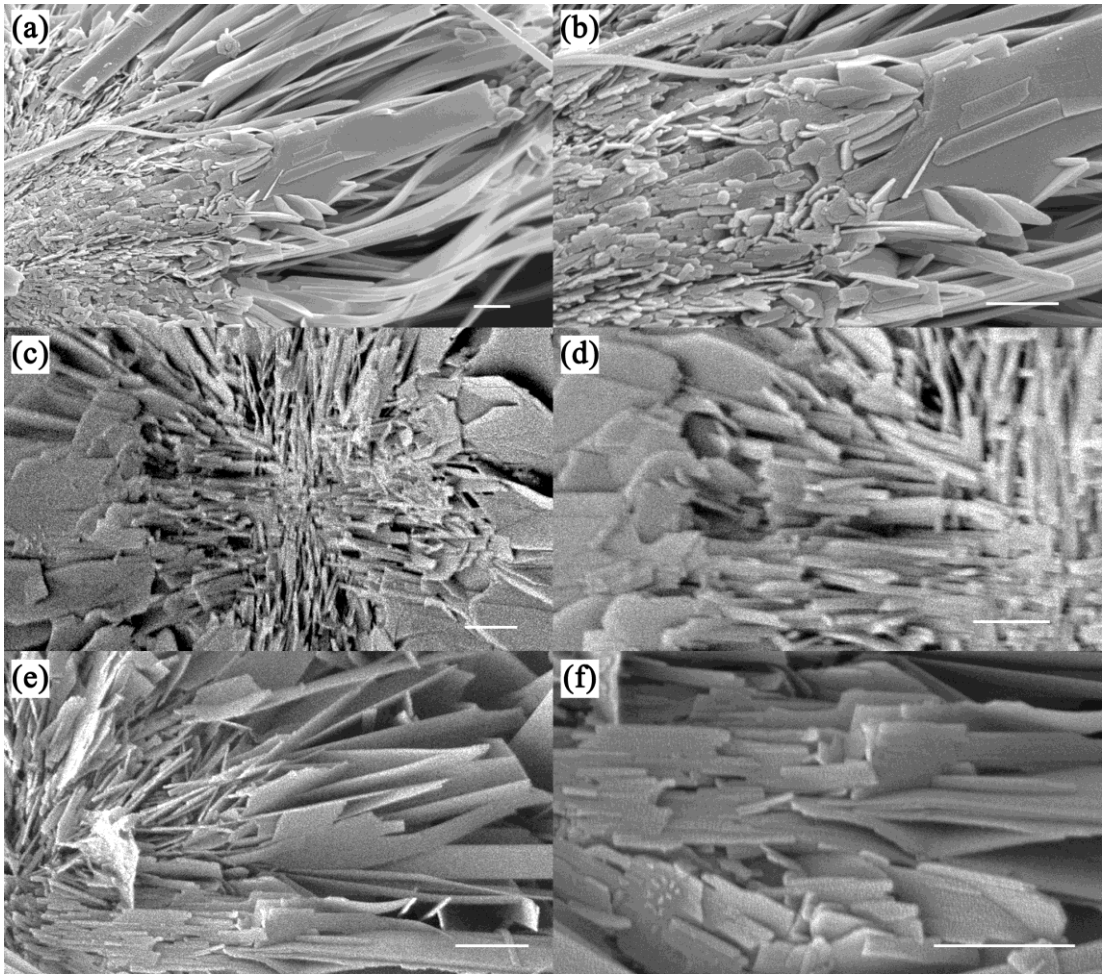

Fig. S4. Cross-section views of three different $Bi_{4.2}K_{0.8}Fe_2O_{9+\delta}$ nanostructures obtained at T_{KOH} = 50 ^{o}C and T_{HT} = 140 ^{o}C. All scale bars are 500 nm.

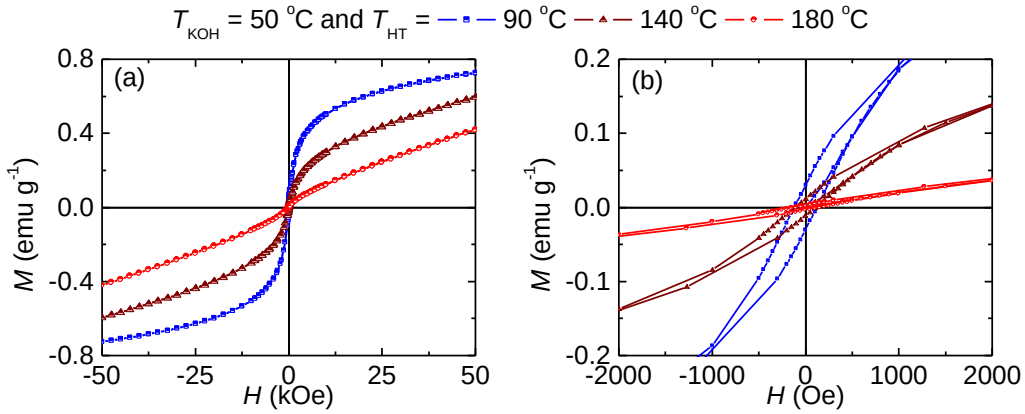

Fig. S5. (a) *M*–*H* curves measured at 10 K for the samples fabricated at T_{KOH} = 50 °C and different T_{HT} (T_{HT} = 90 °C, 140 °C, and 180 °C, respectively). (b) The corresponding enlarged view for the low-field range.

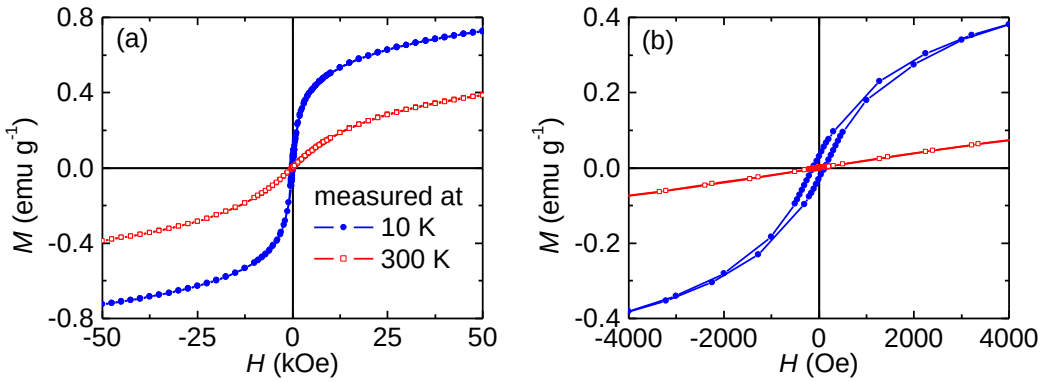

Fig. S6. (a) The comparison of the *M*–*H* curves measured at 300 K and 10 K for the $Bi_{4.2}K_{0.8}Fe_2O_{9+\delta}$ nanostructures obtained at T_{KOH} = 50 °C and T_{HT} = 90 °C. (b) The corresponding enlarged view for the low-field range.

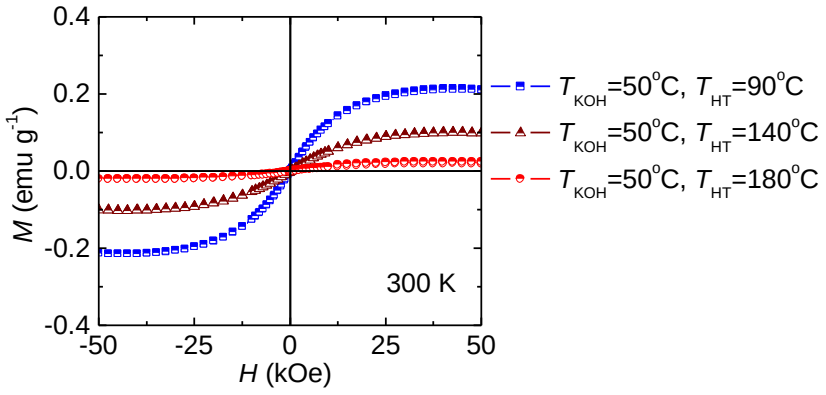

Fig. S7. Ferromagnetic-like signals at 300 K for the samples obtained at T_{KOH} = 50 °C and different T_{HT} (T_{HT} = 90 °C, 140 °C, and 180 °C, respectively), in which the antiferromagnetic and paramagnetic contributions calculated by a linear fitting of the *M*–*H* curves in high magnetic field range are deducted.